

RESEARCH ARTICLE

Modeling flow through tubes and annuli with liquid-infused surfaces for enhanced stability of the fluid-fluid interface

Sebastian Zimmermann¹ | Ellen Bold² | Egbert Oesterschulze² |
 Munehiro Chijiwa^{3,4} | Mareike Schäfer^{3,4} | Johannes L'huillier^{3,4} |
 Clarissa Schönecker¹ 

¹Department of Mechanical and Process Engineering, Rheinland-Pfälzische Technische Universität Kaiserslautern-Landau (RPTU), Kaiserslautern, Germany

²Department of Physics, Rheinland-Pfälzische Technische Universität Kaiserslautern-Landau (RPTU), Kaiserslautern, Germany

³Photonik-Zentrum Kaiserslautern e.V., Kaiserslautern, Germany

⁴Research Center OPTIMAS, RPTU Kaiserslautern-Landau, Kaiserslautern, Germany

Correspondence

Clarissa Schönecker,
 Rheinland-Pfälzische Technische Universität Kaiserslautern-Landau (RPTU), D-67663 Kaiserslautern, Germany.
 Email: c.schoenecker@mv.rptu.de

Funding information

Deutsche Forschungsgemeinschaft, Grant/Award Number: 467661067

Abstract

Superhydrophobic (SHS) and liquid-infused surfaces (LIS) have shown great potential in various engineering applications. Due to their heterogeneous surface properties, a mathematical description of the flow behavior along such surfaces is challenging. Circular textured surfaces are of particular importance. They are modeled as either axially traversed tubes or annuli consisting of no-slip walls that are padded with rotationally symmetric finite-shear regions. The latter represents a viscous interaction zone with a second fluid, assumed with layer thickness zero. Zimmermann and Schönecker provide analytical equations that describe the flow field and effective slip length for such geometries. They are applicable to Newtonian fluids of arbitrary viscosity ratio. This article emphasizes the development of principles and guidelines for the design of SHS and LIS to enhance sliding effects, based on these analytical models. The approach presented here facilitates a geometric evaluation of slippery circular surfaces, aiming to offer insights for the design. Through this research, the potential for significant energy savings and enhanced fluid transport performance can be realized, contributing to the development of more efficient fluid engineering systems.

1 | INTRODUCTION

Superhydrophobic (SHS) and liquid-infused-surfaces (LIS) show enormous potential in many fluid mechanical and process engineering applications [1]. For example, they reduce the pumping efforts required for fluid transport [2] or enhance multi-phase flow in membrane processes. The effect is based on the confinement of lubricant/gas along an otherwise no-slip wall, which allows the fluid to partially slide along the surface. To maximize this sliding effect, air is often selected due to its low viscosity. Because the air covered regions may generate no considerable friction to the traversing fluid flow, they are often modeled to be no-shear patterns on otherwise no-slip walls. However, the practical application of such

This is an open access article under the terms of the [Creative Commons Attribution](https://creativecommons.org/licenses/by/4.0/) License, which permits use, distribution and reproduction in any medium, provided the original work is properly cited.

© 2024 The Authors. *Proceedings in Applied Mathematics & Mechanics* published by Wiley-VCH GmbH.

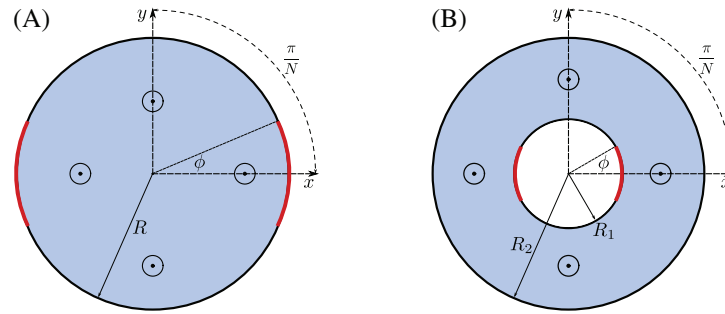


FIGURE 1 Schematic illustration of the discussed geometry [1]. (A) Slippery pipe illustrated as a cross-section in the x, y -plane with flow direction along Z coordinate. Black edges are no-slip walls, red circular arcs represent slip boundaries. (B) Same as in (A) but for an annular pipe containing said shear boundary parts on its inner wall at $|z| = R_1$.

surfaces is hampered by low stability of these air inclusions, endangering these boundary parts to collapse. This must be avoided, since it significantly reduces the desired sliding effect. A potential remedy for this problem is to use oils or other lubricants (LIS) instead of air. However, the assumption of perfect slippage along these lubricated regions fails, as there is a noticeable viscous interaction due to the increased viscosity. Therefore, alternative models are needed that use finite-shear (instead of no-shear) regions to account for these frictional effects. In order to optimize the desired properties of SHS and LIS, appropriate design instruments are necessary. Analytical tools are an important modeling foundation. They enable the description of the flow dynamics and allow conclusions to be drawn about optimization potentials. Furthermore, important parameters can be derived from them, which are of elementary importance for numerical simulations. With the explicit analytical models presented by Zimmermann and Schönecker [1], it is possible to calculate potential energy savings due to sliding effects for SHS and LIS. The models are based on a superposition technique [3] that combines known solutions for no-slip/no-shear mixed-boundary value problems with a flow that represents the presence of a secondary entrapped fluid. Section 2 first presents the analytical expressions for the flow field and the effective slip length derived in literature. [1]. The latter corresponds to an effective boundary condition characterizing the effect induced by the shear patterns. All expressions are valid for any Newtonian fluid of arbitrary viscosity and therefore go beyond the vanishing influence of air viscosity that is often employed in literature [4, 5]. Section 3 then uses these models to quantify and consequently evaluate the pipe geometries investigated in dependence of the flow field and the effective slip length. With that, we present powerful tools to simply assess and understand the geometry of SHS and LIS to make them more energy-efficient.

2 | UNDERLYING MODEL

This work is particularly concerned with pipes and annuli that contain textured walls, see Figure 1.

Such surfaces are commonly modeled as mixed-value boundary problems [6]. The wall areas are conventional no-slip boundaries. The influence of the patterning, and in particular the influence of the second immiscible fluid, is abstracted as a shear boundary condition, illustrated as red circular arcs in Figure 1A and B. It is common to model these areas as so-called no-shear edges. This means that no shear stress is transmitted along these boundary regions, that is, no viscous interaction takes place. This is equivalent to perfect slippage along these areas, which corresponds to an infinite local slip length. Although the no-shear assumption is a quite reasonable approximation of the viscous interaction of trapped air and water, it fails for oils and other lubricants. The models derived in literature [1] overcome this gap and implement finite local slip lengths along the shear boundary regions using a superposition technique. For this purpose, available no-shear equations were superposed with a suitable solution representing the viscous influence along the interface. The results are analytical models that describe the flow field of SHS and LIS tubes or annular pipes with rotationally symmetric finite-shear boundary parts completely as a function of geometry, the viscosity ratio of both fluids and a local slip length. The latter is a parameter defined in the center of the interface. In order to maximize the desired properties of SHS and LIS, such as the reduction of flow resistance, numerous micro- and nanostructures are typically incorporated into the surface. However, since these are much smaller than the general geometry, full numerical resolution is often not feasible. The remedy is an effective boundary condition, smearing out the average boundary effect over the entire respective wall or

boundary. In the case of SHS and LIS, the implementation in (numerical) models is performed with the aid of the effective slip length λ_{eff} using the Navier-slip condition. λ_{eff} is an artificial additional surface depth where the velocity profile of the fluid flow can be linearly extrapolated to zero. With that, the surface loses its exact geometric configuration but retains its mean slippage properties. Thus, it is an important input quantity for numerical studies of microstructured surfaces and can be extracted from analytical models. Furthermore, it is a fundamental quantity for the analytical quantification of slip effects and therefore constitutes the foundation for the geometric optimization of such surfaces. The following sections introduce the analytical models derived in literature [1] for the velocity field and the effective slip length of LIS tubes (Section 2.1) and annular LIS pipes (Section 2.2). For a more in-depth derivation see literature [1].

2.1 | SHS and LIS tube

A very important source for the mathematical description of flows along SHS is the work of Philip [4] from 1972. He provides numerous analytical solutions for a number of mixed-value boundary problems, including pressure-driven axial flow through a pipe with rotationally symmetric no-shear regions along the outer wall. As mentioned, Philip's solution does not consider viscous interaction at the fluid-fluid interface. To overcome this limitation, Philip's solution is superposed with a classical Poiseuille flow. Incorporating appropriate constraints [1] yields

$$\bar{w}(\bar{z}) = \frac{1}{4}(\bar{R}^2 - |\bar{z}|^2) + \alpha \frac{\bar{R}^2}{N} \tau(\bar{z}), \quad (1)$$

for the velocity along the Z axis. It is normalized with respect to $w(\bar{z}) \mu / (s R_0^2)$, where $s = -\Delta p$ is the negative axial pressure gradient, R_0 a characteristic radial scale and μ the dynamic viscosity of the bulk fluid. $\bar{z} = z/R_0 = \bar{x} + i \bar{y}$ is the normalized complex coordinate and \bar{R} the dimensionless outer pipe radius. N denotes the number of shear boundary parts. Equation 1 consists of a rotationally symmetric first term (Poiseuille flow) and an asymmetric second term, the latter describing the impact induced by the finite-shear boundary regions, which is governed by

$$\tau(\bar{z}) = \Im \left[\cos^{-1} \left(\frac{\cos(\kappa(\bar{z}))}{\cos\left(\frac{\theta}{2}\right)} \right) - \kappa(\bar{z}) \right], \quad \kappa(\bar{z}) = -\frac{i}{2} \ln \left(\frac{\zeta}{\bar{R}^N} \right) = -\frac{iN}{2} \ln \left(\frac{\bar{z}}{\bar{R}} \right), \quad (2a,b)$$

with angle θ being a measure for the shear fraction. In fact, θ/π denotes the proportion of the total wall surface occupied by finite-shear boundary parts. The complex coordinate $\zeta = z^N$ is the result of a conformal mapping performed by Philip. The coefficient α can be interpreted as an imperfection factor, steering the magnitude of the asymmetric term in dependence of the normalized local slip length $\tilde{\lambda} = \lambda/R_0$ at the slit center $\bar{z} = \bar{R} + i 0$. It is given as

$$\alpha = \frac{\tilde{\lambda}N}{\tilde{\lambda}N + 2\bar{R}\tau(\bar{z})}, \quad (3)$$

with $\tau(\bar{z})$ being the function $\tau(\bar{z})$ evaluated at the slit center. The coefficient is, apart from $\tilde{\lambda}$, purely dependent on geometric parameters. Thus, if the local slip length is known, the viscous influence of the fluid-fluid interface on the bulk flow field is straightforward to quantify. An analysis of α shows furthermore, that $\tilde{\lambda} = 0$ leads to an imperfection coefficient of $\alpha = 0$, so Equation 1 reduces to the classical Poiseuille flow with a uniform no-slip wall at $|\bar{z}| = \bar{R}$. However, for an infinite local slip length, α converges to 1. Accordingly, the velocity field converges to the no-shear solution provided by Philip [4]. With the velocity field as a function of $\tilde{\lambda}$, the effective slip length can now be derived. Based on literature [1], it is given by

$$\tilde{\lambda}_{\text{eff}} = 2 \bar{w}_{\text{avg}}(\bar{R}). \quad (4)$$

Equation 4 follows from deriving Poiseuille equation with a Navier-slip boundary condition at $|\bar{z}| = \bar{R}$ instead of implementing no-slip, as is usually done. It is now sufficient to find the averaged velocity \bar{w}_{avg} at the wall at $|\bar{z}| = \bar{R}$ based on Equation 1. It is easy to see that the only rotationally asymmetric part in Equation 1 is $\tau(\bar{z})$. Averaging that term along the boundary involves using the integral identities given by literature [7]. Subsequently inserting this mean value into flow

field equation, evaluating at $|\tilde{z}| = \tilde{R}$, gives the normalized effective slip length

$$\tilde{\lambda}_{\text{eff}} = \frac{\lambda_{\text{eff}}}{R_0} = \alpha \frac{2}{N} \ln \left(\sec \left(\frac{\theta}{2} \right) \right). \quad (5)$$

The detailed derivation of the normalized effective slip length for the finite-shear solution (Equation 5) can be found in literature [1]. For $\tilde{\lambda} \rightarrow \infty$, Equation 5 converges to the no-shear solution provided by Lauga and Stone [8], as expected. Accordingly, the no-shear solution represents the idealized case for non-existent viscous interaction along the fluid-fluid interface of the these finite-shear model.

While the no-shear models are well suited for calculating SHS with enclosed air, they reach their limits when more viscous fluids are entrapped. Therefore, these finite-shear models are to be understood as an extension, broadening the spectrum of applicability to more general cases such as LIS.

2.2 | Annular SHS and LIS pipe

Another fundamental case of circular geometries are concentric annuli, see Figure 1B. Darren Crowdy [5] has derived models for pressure-driven axially traversed annuli containing rotationally symmetrical slits on the inner wall. These also have mixed-value boundaries, as in Philip's case, consisting of no-slip walls and no-shear patterning. Superposing these solutions with a Poiseuille flow, using appropriate constraints [1], yields

$$\bar{w}(\tilde{z}) = \frac{1}{4} \left((1 - |\tilde{z}|^2) + 2\beta_1 \Re(H(\zeta)) - \beta_2 (1 - \tilde{R}_1^2) \frac{\ln(|\tilde{z}|)}{\ln(\tilde{R}_1)} \right), \quad (6)$$

where the outer radius of the annulus is set to be 1 [5]. The first term in brackets is again a classical Poiseuille flow and the last being an part of an annular Poiseuille solution. Both are rotationally symmetric. The asymmetric term (the middle expression in the parenthesis) represents the shear impact from the slit regions and is governed by $\Re(H(\zeta))$, which denotes the real part of an analytic function $H(\zeta)$ defined as

$$H(\zeta) = \frac{1}{N} \int_{-1}^{\zeta} \left[\tilde{R}_1^2 - M \left(\frac{P\left(\frac{\zeta'}{q}, q\right) P\left(\frac{\zeta'}{q}, q\right)}{P\left(\frac{\zeta'}{a}, q\right) P\left(\frac{\zeta'}{a}, q\right)} \right)^{1/2} \right] \frac{d\zeta'}{\zeta'}. \quad (7)$$

where $a = \tilde{R}_1^N e^{i\theta}$ and $q = \tilde{R}_1^N$. Angle $\theta = \phi N$ is defined in the same way as in Section 2.1. The variable $\zeta = z^N$ is again the transformed complex coordinate. M is a scaling factor imposing no-slip at the appropriate portions of the inner wall at $|\tilde{z}| = \tilde{R}_1$ and is given as

$$M = \frac{\frac{(1-\tilde{R}_1^2)}{4} + \frac{1}{2}\tilde{R}_1^2 \ln(\tilde{R}_1)}{S}, \quad S = \frac{1}{2N} \int_{-1}^{-q} \left(\frac{P\left(\frac{\zeta}{q}, q\right) P\left(\frac{\zeta}{q}, q\right)}{P\left(\frac{\zeta}{a}, q\right) P\left(\frac{\zeta}{a}, q\right)} \right)^{1/2} \frac{d\zeta}{\zeta}. \quad (8a,b)$$

$P(\zeta, q)$ is the so-called prime function for the concentric annulus. It is given as a convergent infinite product for any $\zeta \neq 0$

$$P(\zeta, q) = (1 - \zeta) \prod_{n=1}^{\infty} (1 - q^{2n} \cdot \zeta)(1 - q^{2n}/\zeta), \quad 0 \leq q < 1. \quad (9)$$

For more information on the concept of prime functions, see [9]. The two coefficients β_1 and β_2 weight the influence of the second and third term in brackets in Equation 6, with $\beta_1 + \beta_2 = 1$. Accordingly, they control whether the no-shear or no-slip character of the solution dominates. In this sense, they are comparable to the imperfection factor α in Equation 1

from Section 2.1. They are defined as

$$\beta_1 = \frac{\tilde{\lambda} \left(\tilde{R}_1^2 + 2\tilde{R}_1^2 \ln \left(\frac{1}{\tilde{R}_1} \right) - 1 \right)}{\left[\tilde{R}_1^2 \tilde{\lambda} - \tilde{\lambda} + \tilde{R}_1 \ln \left(\frac{1}{\tilde{R}_1} \right) (\tilde{R}_1^2 - 2\Re(H(q)) + 2\tilde{\lambda}\tilde{R}_1 - 1) \right]}, \quad \beta_2 = (1 - \beta_1). \quad (10a,b)$$

$H(q)$ denotes the analytic function $H(\zeta)$ evaluated at the slit center, which corresponds to q . Both, β_1 and β_2 are solely dependent on geometry parameters, apart from $\tilde{\lambda}$, which is to be determined in dependence on the viscous interface interaction along the interface. For $\lambda = 0$, β_1 becomes zero and $\beta_2 = 1$, so that the velocity field describes a classical annular Poiseuille flow with no-slip boundary condition on both walls, $|\tilde{z}| = \tilde{R}$ and $|\tilde{z}| = 1$. For infinite local slip lengths the matter is exactly opposite and the solution from Equation 6 corresponds to the no-shear flow field derived by Crowdy [5]. As in Section 2.1, the effective slip length can similarly be obtained for an annular axial flow, based on Equation 6. It is given by

$$\tilde{\lambda}_{\text{eff}} = \frac{\lambda_{\text{eff}}}{R_0} = -\frac{4\tilde{R}_1 \ln(\tilde{R}_1) \tilde{w}_{\text{avg}}}{(1 - \tilde{R}_1^2 - 4\tilde{w}_{\text{avg}} + 2\tilde{R}_1^2 \ln(\tilde{R}_1))}. \quad (11)$$

which again follows from implementing the Navier-slip condition in the Poiseuille flow derivation, this time on the inner wall for the concentric annulus case. Similar to before, the real part of the asymmetric function $H(\zeta)$ must be averaged along the inner wall at $|\tilde{z}| = \tilde{R}_1$, since the remaining velocity field is rotationally symmetric. If plugged into 6 and evaluated at $|\tilde{z}| = \tilde{R}_1$, it yields the averaged velocity w_{avg} . Inserting that into Equation 11 finally results in

$$\tilde{\lambda}_{\text{eff}} = \frac{\lambda_{\text{eff}}}{R_0} = \tilde{R}_1 \ln(\tilde{R}_1) \beta_1 \frac{I_{-1} \ln(\tilde{R}_1) - 2S}{I_{-1} \ln(\tilde{R}_1) \beta_1 - 2S(\beta_1 - 1)}, \quad (12)$$

with [5]

$$I_{-1} = \frac{1}{2\pi i} \oint_C \left(\frac{P\left(\frac{\zeta}{q}, q\right) P\left(\frac{\zeta}{q}, q\right)}{P\left(\frac{\zeta}{a}, q\right) P\left(\frac{\zeta}{a}, q\right)} \right)^{1/2} \frac{d\zeta}{\zeta}, \quad (13)$$

C is any closed circle inside the annulus $q < |\zeta| < 1$ enclosing the origin, S and $P(\zeta, q)$ are given in Section 2.2. For a more in-depth derivation, see literature [1]. On closer inspection, the effective slip length is therefore primarily a function of geometric parameters. However, due to its dependence on the local slip length, the viscous interactions is also taken into account. For $\tilde{\lambda} \rightarrow \infty$ Equation 12 again transitions to the no-shear solution given by Crowdy [5] and is zero for $\tilde{\lambda} = 0$, as it should be. Accordingly, both no-slip and no-shear solutions can be understood as extreme values of the equation derived in literature [1]. In between lies a wide spectrum of slip conditions that make it possible to represent non-idealized viscous interface interactions as in the example of LIS.

3 | EFFECTS OF SURFACE DESIGN AND THEIR IMPLICATIONS

The geometry and the fluid properties have great influence on the slippage effects of SHS and LIS. More precisely, they depend on the surface fraction of the shear slits, the number of shear boundaries N , the general tube geometry, the local slip length λ and the viscosity ratio of the fluids under consideration. With regard to the geometry, it is therefore particularly important to determine those configurations that maximize the desired properties of the surface, such as drag reduction. The analytical models from Section 2 play a crucial role in identifying parameter combinations that maximize these effects, such as the effective slip length. They then allow the formulation of design guidelines for the layout of SHS and LIS and contributing to the development of sustainable fluid engineering systems. Figure 2 illustrates contour plots of the axial velocity field, where 60% of the pipe wall is occupied by finite-shear slits of different widths. A local slip length at the slit center of $100 \mu\text{m}$ is assumed. The velocity field provides important information about local velocity gradients and the associated shear stresses within the flow. An oscillating contour pattern can be seen along the patterned walls. This

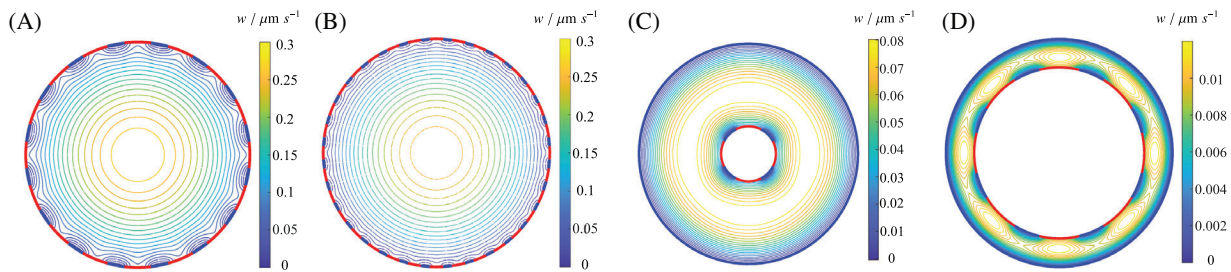


FIGURE 2 Contour plot of the axial velocity field of pipes and annuli with outer radius $R = 1000 \mu\text{m}$ containing N rotationally symmetric finite-shear slits occupying 60% of a wall. The local slip length at the slit center is set to be $100 \mu\text{m}$ in all cases. (A) $N = 16$ with an circular slit length of approx. $235 \mu\text{m}$ each. (B) $N = 32$ with an circular slit length of approx. $117 \mu\text{m}$ each. (C) $N = 4$ with an circular slit length of approx. $235 \mu\text{m}$ each. (D) $N = 8$ with an circular slit length of approx. $350 \mu\text{m}$ each.

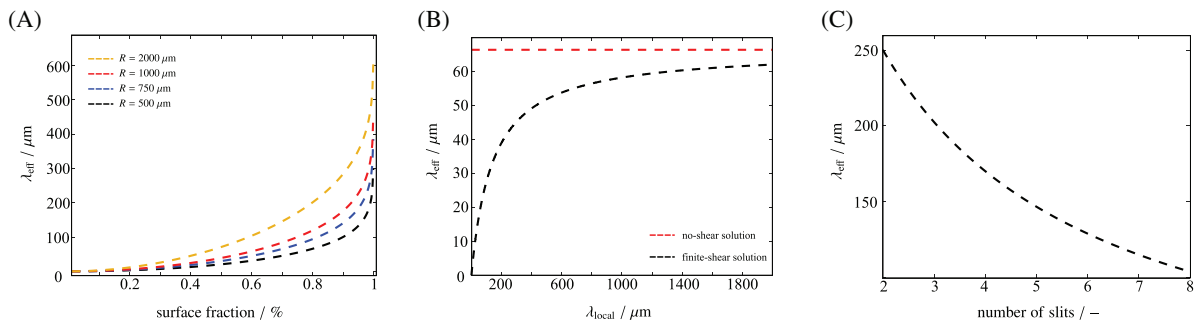


FIGURE 3 Various plots illustrating the graph of the effective slip length (in μm) for a pipe flow containing rotationally symmetric finite-shear slits as a function of tunable parameters. (A) Effective slip length as a function of the surface fraction occupied by finite-shear slits. Analysis for pipe radii 500, 750, 1000, and $2000 \mu\text{m}$. Assuming: $N = 16$, $\lambda = 1000 \mu\text{m}$. (B) Effective slip length as a function of the local slip length λ at the slit center. Comparison between no-shear [4] and finite-shear solution. Assuming: $N = 8$, $\theta = 0.6\pi$, $R = 500 \mu\text{m}$. (C) Effective slip length depending on the number of finite-shear slits N keeping $\theta = 0.6\pi$ constant. Assuming: $\lambda = 1000 \mu\text{m}$, $R_0 = 1000 \mu\text{m}$.

obviously arises from the alternating no-slip and finite-shear regions, with the transition points in-between. Especially the comparison of figure 2A and B reveals an interesting pattern. Both geometries have the same outer radius and both walls are 60% occupied by finite-shear grooves (all with the same slip length). However, it can be clearly seen that the range of the groove influence on the bulk flow is greater with 16 grooves than with twice the number of grooves. In the latter case, the influence is almost completely locally bound. This finding allows immediate conclusions to be drawn regarding the effective slip length, as will be further discussed below.

For more precise quantification, practical examples are now used to illustrate a simple method for optimizing patterned surfaces.

Figure 3 shows different ways to optimize SHS and LIS pipes based on the Equation 5. Part (a) shows different effective slip lengths for an increasing surface fraction of finite-shear boundary parts for different pipe radii. For low surface fractions, the relationship is almost linear, but λ_{eff} then increases disproportionately for a surface fraction above 60%, which provides crucial insight for basic SHS and LIS design guidelines. Clearly, the influence on the bulk flow is greater with decreasing pipe radius. In addition, Figure 3B shows the asymptotic behavior of the finite-shear model provided in literature [1] (black dashed line) to Philip's no-shear solution [4] (red dashed line) with increasing local slip length. This clearly shows that the no-shear solution is the limit of the more general case of finite-shear. Finally, part (c) illustrates the progression of λ_{eff} with increasing number of finite-shear patterns N , while the surface fraction remains constant. It can be clearly seen that the smallest possible number of slits is advantageous for the scenario under consideration. However, keeping N minimal, the interfaces must then span a greater distance, which makes the wetting state less stable overall. Accordingly, this is an optimization problem of both influencing factors. These simple evaluations already show the great importance of analytical expressions for the effective sliding length. As previously mentioned, λ_{eff} is also of great importance for CFD simulations and can be implemented there as a simple boundary condition to represent a geometric complexity that otherwise cannot be numerically resolved.

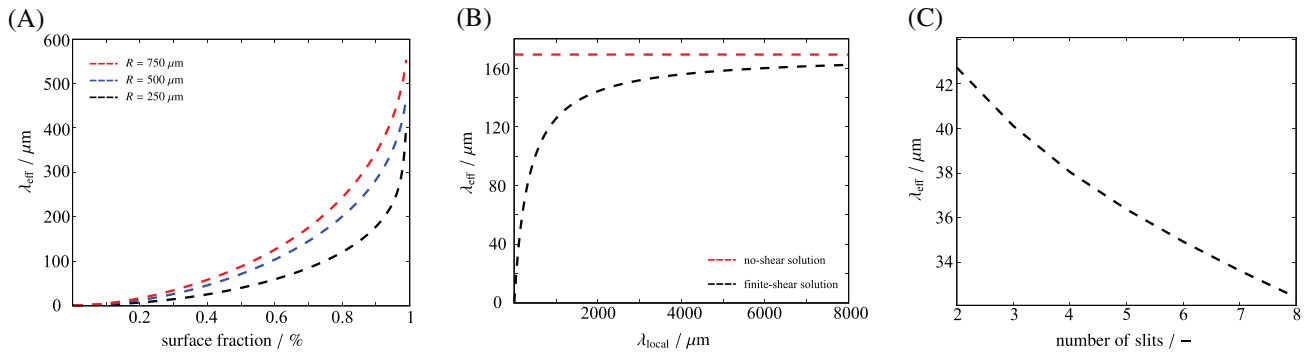


FIGURE 4 Various plots illustrating the graph of the effective slip length (in μm) for an annular pipe containing N finite-shear slits at the inner wall as a function of certain tunable parameters. (A) Effective slip length as a function of the surface fraction occupied by finite-shear slits. Analysis for inner radii R_1 being 250, 500, and $750 \mu\text{m}$. Assuming: $N = 4$, $\lambda = 1000 \mu\text{m}$. (B) Effective slip length as a function of the local slip length λ at the slit center. Comparison between no-shear [5] and finite-shear solution. Assuming: $N = 4$, $\theta = 0.6\pi$, $R_2 = 1000 \mu\text{m}$ and $R_1 = 750 \mu\text{m}$. (C) Effective slip length depending on the number of finite-shear slits N keeping $\theta = 0.6\pi$ constant. Assuming: $\lambda = 100 \mu\text{m}$, $R_0 = 1000 \mu\text{m}$, and $R_2 = 800 \mu\text{m}$.

Similar to before does figure 4 show different ways to optimize annular SHS and LIS tubes based on Equation 12. Part (a) shows different effective slip lengths for an increasing surface fraction of finite-shear boundary parts for three different inner pipe radii keeping the outer radius constant. Again, for very low surface fractions, a roughly linear progression is detected. Finally, the effective slip length grows increasingly steep, as it did for the slippery pipe. Figure 3B shows the asymptotic behavior of the finite-shear model provided in literature [1] (black dashed line) to Crowdy's no-shear solution (red dashed line) with $\tilde{\lambda} \rightarrow \infty$. Finally, part (c) again illustrates the progression of λ_{eff} with increasing number of finite-shear slits N , keeping the surface fraction constant. It can be clearly seen that the smallest possible number of grooves is advantageous for the scenario under consideration, as for the pipe case.

4 | CONCLUSIONS

This article shows simple methods for the geometric design of circular SHS and LIS, based on analytical models for calculating pressure-driven flow fields and the effective slip length of axially traversed pipes and annuli with rotationally symmetric finite-shear boundary parts [1]. These models extend previous approaches commonly used in literature, which assume perfect slip along the fluid-fluid interface and thus do not take into account several influencing factors important for modeling SHS and LIS. Thus, the presented design methods enable the modeling of a wide spectrum of textured surfaces going beyond classical SHS. Based on these models, first qualitative conclusions about the global influence of the finite-shear grooves were drawn using contour plots of the velocity fields, as given in Equations 1 and 12. It was found that the influence of the shear boundary regions becomes more and more local with increasing number of grooves, that is, they influence the global flow less and less. This follows natural intuition, after all, the shear edges are repeatedly disturbed by no-slip intermediate pieces. It was then illustrated how important elementary correlations can be derived with simple considerations regarding the behavior of λ_{eff} , as certain parameters such as N , θ , and λ_{local} are varied. From these analyses, the tendency towards a minimum number of grooves can first be confirmed. Figure 3B and 4B obviously show that the effective slip length grows with increasing local slip. Finally, different tube radii or inner radii of the annulus were considered in Figures 3A and 4A, from which it can be concluded that with decreasing channel size the effective slip length increases significantly. In other words, the effects along the slippery wall become increasingly dominant compared to the bulk flow dynamics.

Overall, the presented methods allow to assess and better understand patterned surfaces and represent elementary tools for the design and optimization of SHS and LIS.

ACKNOWLEDGMENTS

We kindly acknowledge support by the Deutsche Forschungsgemeinschaft (DFG, German Research Foundation) - Project-ID 467661067.

Open access funding enabled and organized by Projekt DEAL.

ORCID

Clarissa Schönecker  <https://orcid.org/0000-0003-1826-9801>

REFERENCES

1. Zimmermann, S., & Schönecker, C. (2024). Analytical models for pressure-driven Stokes flow through superhydrophobic and liquid-infused tubes and annular pipes. *Journal of Fluid Mechanics*, 978, A20.
2. Rothstein, J. P. (2010). Slip on superhydrophobic surfaces. *Annual Review of Fluid Mechanics*, 42, 89–109.
3. Schönecker, C. (2014). Influence of the enclosed fluid on the flow over a microstructured surface in the Cassie state. *Journal of Fluid Mechanics*, 740, 168–195.
4. Philip, J. R. (1972). Flows satisfying mixed no-slip and no-shear conditions. *Zeitschrift für angewandte Mathematik und Physik ZAMP*, 23, 353–372.
5. Crowdy, D. G. (2021). Superhydrophobic annular pipes: A theoretical study. *Journal of Fluid Mechanics*, 906, A15.
6. Schönecker, C., & Hardt, S. (2013). Longitudinal and transverse flow over a cavity containing a second immiscible fluid. *Journal of Fluid Mechanics*, 717, 376–394.
7. Philip, J. R. (1972). Integral properties of flows satisfying mixed no-slip and no-shear conditions. *Zeitschrift für angewandte Mathematik und Physik ZAMP*, 23, 960–968.
8. Lauga, E., & Stone, H. (2003). Effective slip in pressure-driven Stokes flow. *Journal of Fluid Mechanics*, 489, 55–77.
9. Crowdy, D. G. (2020). *Solving problems in multiply connected domains*. Society for Industrial and Applied Mathematics.

How to cite this article: Zimmermann, S., Bold, E., Oesterschulze, E., Chijiwa, M., Schäfer, M., L’huillier, J., & Schönecker, C. (2024). Modeling flow through tubes and annuli with liquid-infused surfaces for enhanced stability of the fluid-fluid interface. *Proceedings in Applied Mathematics and Mechanics*, 24, e202300140.
<https://doi.org/10.1002/pamm.202300140>